Smart Structures and Systems, *Vol. 28, No. 1 (2021) 13-28*
https://doi.org/10.12989/sss.2021.28.1.013

Critical coupling span number in high-speed railway simply supported beam bridge

Yuntai Zhang [1a], Lizhong Jiang [1,2b], Wangbao Zhou*[1], Yulin Feng [1c], Xiang Liu [1d] and Zhipeng Lai [1e]

[1] *School of Civil Engineering, Central South University, Changsha 410075, China*
[2] *National Engineering Laboratory for High Speed Railway Construction, Changsha 410075, China*

(*Received December 23, 2019, Revised March 18, 2021, Accepted March 24, 2021*)

Abstract. In long-distance railways, some particular spans of high-speed railway simply supported beam bridges (HSRSBs) are commonly selected as the target structure. The target structure is the part of interest for the study and intended to be analyzed. Due to longitudinal constraints of the track system, the target structure is tightly coupled with other spans within certain range, and is affected by the coupled spans under longitudinal earthquake condition. A massive amount of time-consuming computation is required to determine the coupling span number using current finite element models. In an effort to overcome this challenge, an equivalent method for the longitudinal constraints of the track system is proposed, which greatly reduces the complexity of finite element model while retaining calculation precision. The coupling span number was determined by seismic analyses of a large number of cases using equivalent finite element models. Moreover, the influence of pier height and bottom pier stiffness on coupling span number was studied. Based on the relationship between the equivalent boundary sensitivity critical point and coupling span number, a method to quickly obtain coupling span number of the target structure in arbitrary HSRSB was constructed.

Keywords: coupling effect; critical coupling span number; equivalent model; spring-mass system

1. Introduction

In the previous studies of the dynamic response of the high-speed railway simply supported beam bridges (HSRSBs), the few spans with typical structures or specific foundation condition were selected as the target structure for analysis in detail (Ju 2012, Montenegro *et al*. 2016, Kang *et al*. 2017, Gou *et al*. 2018, Wei *et al*. 2019, 2020). Based on this modeling principle, the vehicle-track-bridge system had also been widely studied (Liu and Ni 2018, Jiang *et al*. 2019a, Liu *et al*. 2019a). However, it should be noted that a significant amount of the existing literature on the calculation model for HSRSB has clear shortcomings in boundary processing, in which the track constraint effects at the HSRSB model boundaries are neglected.

With continuous welded rail (CWR) has been widely used in high-speed railway bridges, considerable researches have been conducted to investigate the track constraint effects (Lai and Ho 2014, Feng *et al*. 2019, Yan *et al*. 2019). These studies mainly focus on bridge-track interaction (Zhang *et al*. 2020) or train-track interaction (Zhai *et al*. 2019, Montenegro *et al*. 2020a, b). Maragakis *et al*. (1996) investigated the effect of tracks on the dynamic performance of Strawberry Park ballasted bridge. According to the experimental results, significant vibration is transmitted to the adjacent subgrade when a track exists in the edge of the bridge; the fundamental frequencies of structures in longitudinal, transverse, and vertical directions all decline to some extents when tracks are cut off. Based on the experimental research and theoretical analysis, Iemura *et al*. (2004) believed that the rail constraint has a certain impact on the energy dissipation capacity of the seismic isolation device. Toyooka *et al*. (2005) found that the effect of the track constraint on the longitudinal natural frequency of railway bridges with vibration absorption and isolation devices was not negligible. Jiang *et al*. (2019b) found that the subgrade part of high-speed railway simply supported beam bridge-track structure system has a critical rail length by evaluating the natural vibration characteristics under different interlayer stiffness and lengths of rails at different subgrade parts. Therefore, due to the longitudinal constraining effect of the track system, the target structure is tightly coupled with other spans within a certain number, and the dynamic characteristics of the target structure would be affected by the coupling spans. In order to establish proper calculation model for the target structures, it is necessary to determine the coupling span number of target structures.

It is not advisable to directly establish the calculation models to obtain the coupling span number because of the massive dynamic response computations of a large number of bridges with different spans. The main object of the study is the target structure, hence most of these calculations are

*Corresponding author, Professor,
E-mail: zhouwangbao@163.com
[a] Ph.D., E-mail: zhangyuntai@csu.edu.cn
[b] Professor, E-mail: lzhjiang@csu.edu.cn
[c] Dr., E-mail: fylin119@csu.edu.cn
[d] Ph.D., E-mail: liuxiang2017@csu.edu.cn
[e] Dr., E-mail: laizhipeng2016@163.com

ISSN: 1738-1584 (Print), 1738-1991 (Online)

redundant. More importantly, completing the perimeter analysis consumes a lot of time due to numerous computations, which impedes obtaining the target structure coupling span number quickly in future studies on HSRSBs. Hence, the proper equivalence of the model is a reasonable approach to the dynamic analysis of the target structure and the study of coupling span number. In recent years, relevant methods for equivalence have been proposed. Li and Conte (2016) developed a non-linear spring model defined as a single element, denoted as series–parallel spring model, and incorporated it at the cut of each rail to account for the longitudinal support provided. In order to have the seismic behavior of a single superstructure segment not affected by the boundary conditions at the endings, Zanardo *et al*. (2010) placed spring-dashpot elements with stiffness and damping to simulate the boundaries of an infinitely long bridge, according to the studies conducted by Jankowski *et al*. (1998, 2000). In order to study the influence of track slab on the seismic response of the high-speed railway bridge, Zhang *et al*. (2014) established simply supported beam bridge model considering track plate and longitudinal constraint boundary at plate end. In Shan's study (Shan *et al*. 2017), a new coupled vehicle-track-subgrade model is established by the finite-infinite element method, and the infinite elements were employed on the bottom and the right hand side of the subgrade. However, only the equivalent system of single-layer longitudinal continuously component was adopted in most previous research, which is difficult to consider the longitudinal constraint effect of track system with multi-layer longitudinal continuously component. In addition, most previous methods primarily focused on the equivalence of subgrade structures instead of bridge structures, which has little influence on the study of coupling span number. Also, derivation is provided only about the equivalent stiffness while there is no such derivation about the equivalent mass.

In this work, an equivalent method for China Railway Track System II (CRTS II) ballastless track-bridge system was proposed for studying the coupling span number of target structures in HSRSBs. By not affecting the refinement of the target structure model, the other parts of the model could be converted into a spring-mass system connected to the target structure. Thus, an equivalent FE model with similar mechanical characteristics to the original FE model is established, which can greatly reduce the element number. The effect of span number on the seismic response of the target structure is analyzed by calculating large quantities of equivalent FE models for the HSRSB with different span number. The relationship between the disadvantageous span number in the seismic response (N_{NS}) and the span number with maximum magnification (N_{NMM}) was found. Based on the relationship between the coupling span number of the target structure and the critical sensitivity point for the equivalent boundary characteristics, a method (SEBCM) is proposed to quickly calculate the coupling span number of the target structure in HSRSBs using an arbitrary pier height and bottom pier stiffness.

2. Equivalent method for the adjoining structure

Previous studies have shown that the seismic responses of HSRSBs are greatly affected by the track constraints in the longitudinal direction (Li and Conte 2016, Yan *et al*. 2017, Zhang *et al*. 2020). To analyze HSRSBs using CRTSII ballastless track, HSRSB can be divided into the target structure and the adjoining structure in this paper. The target structure is the part of interest for this study. The adjoining structure is divided into the adjoining-subgrade structure and adjoining-bridge structure (Fig. 1). When the adjoining-subgrade structure, adjoining-bridge structure, and target structure are included in the calculation model, the overall calculation amount is huge. Converting the adjoining structure to an equivalent boundary can simplify the calculation model and significantly improve computational efficiency. Since this paper only discusses the longitudinal earthquake excitation, the conversion process is only considered in the longitudinal direction.

As the proposed method is in the preliminary stage, in order to initially study the simplified method proposed, the equivalence of adjoining structure can be studied under the assumption of linear elasticity in this paper. Based on the number of longitudinal connection points in the structure,

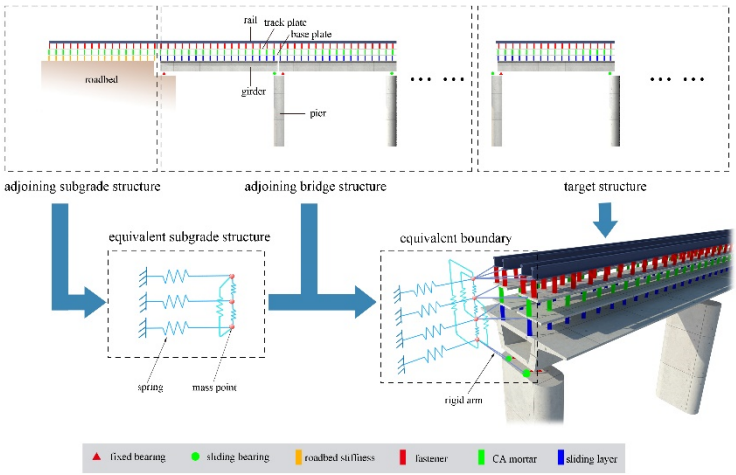

Fig. 1 Converting the adjoining structure to an equivalent boundary

the adjoining-subgrade structure can be converted to an equivalent subgrade structure composed of 3 mass-points and 6 springs, which is connected to the adjoining-bridge structure through three connection points. Similarly, the equivalent subgrade structure and the adjoining-bridge structure can be converted to an equivalent boundary composed of 4 mass points and 10 springs that is then connected to the target structure through four connection points (Fig. 1). The specific meaning of the connection points will be explained in the section 2.1.

The equivalent boundary is more difficult to obtain than the equivalent subgrade structure due to the increased number of connection points, and the equivalence of the adjoining-subgrade structure is a special case of the equivalence for adjoining-bridge structures. Therefore, this chapter only demonstrates the equivalence of adjoining-bridge structures in detail. In order to establish an equivalent boundary system, the complete adjoining-bridge structure is divided into many segments by using the positions of fasteners as the segment demarcation points. The details of equivalence are as follows.

2.1 Equivalence of the initial segment

Based on assumption of linear elasticity and lumped masses, the initial segment of adjoining-bridge structure can be expressed using a spring-mass model with concentrated parameters, where the element longitudinal stiffness is simulated using a spring and mass that is equally divided onto two at the endpoints of the element (Fig. 2). k_{gg}, k_{gd}, k_{dz}, k_z, k_{kj}, k_{sj}, k_{hd}, k_d, k_{fs}, and k_{ss} are the unit longitudinal stiffnesses of the rail, track slab, base slab, girder, fastener, CA mortar layer, sliding layer, pier, fixed bearing, and sliding bearing of CRTSII track system, respectively, and m_{gg}, m_{gd}, m_{dz}, m_z, and m_d are the unit mass of the rail, track slab, base slab, and girder, respectively. Joint points 1, 2, 3, and 4 refer to the points at which the rail, track slab, base slab, and girder, respectively, are connected to the next segment.

According to the equivalent method proposed below, the calculation model (Fig. 2(a)) is equivalent to the equivalent model (Fig. 2(b)). The new model is referred to as the equivalent model for the initial segment and is composed of four mass points and ten springs, wherein $k_{1,1}$ $k_{1,2}$, $k_{1,3}$, and $k_{1,4}$ represent the direct equivalent stiffness, and $k_{1,12}$, $k_{1,23}$, $k_{1,13}$, $k_{1,14}$, $k_{1,24}$, and $k_{1,34}$ represent the indirect equivalent stiffness. $m_{1,1}$, $m_{1,2}$, $m_{1,3}$, and $m_{1,4}$ are the equivalent masses at joint points 1, 2, 3, and 4, respectively. $k_{C,1}$ $k_{C,2}$ and $k_{C,3}$ represent the direct equivalent stiffness of the equivalent subgrade structure, and $k_{C,12}$, $k_{C,23}$, and $k_{C,13}$ represent the indirect equivalent stiffness of the equivalent subgrade structure. $m_{C,1}$, $m_{C,2}$, $m_{C,3}$ are the equivalent masses of the equivalent subgrade structure.

In the equivalent model for the initial segment, the equivalent stiffness and equivalent masses of joint points can be solved using the displacement method.

In solving the equivalent stiffness of point 1, consolidation is conducted on points 2, 3, and 4, and the virtual longitudinal unit displacement is applied to point 1 (Fig. 3(a)). Based on the series/parallel spring connections, the following equation can be obtained

$$\begin{pmatrix} Z_1 & -Z_2 & 0 \\ -Z_2 & Z_3 & -k_{\mathrm{hd}} \\ 0 & 0 & Z_4 \end{pmatrix} \begin{pmatrix} 1-\delta_{12} \\ 1-\delta_{13} \\ 1-\delta_{14} \end{pmatrix} = \begin{pmatrix} k_{C,2}+k_{\mathrm{gd}} \\ k_{C,3}+k_{\mathrm{dz}} \\ k_{\mathrm{fs}}+k_z \end{pmatrix} \quad (1)$$

Where $Z_1 = k_{C,2} + k_{gd} + k_{C,12} + k_{kj} + k_{C,23} + k_{sj}$; $Z_2 = k_{C,23} + k_{sj}$; $Z_3 = k_{C,3} + k_{dz} + k_{C,13} + k_{C,23} + k_{sj} + k_{hd}$; $Z_4 = k_{fs} + k_z + k_{hd}$; $\delta_{12}, \delta_{13}, \delta_{14}$ denote the joint displacement of points 2, 3, and 4 caused by the unit displacement of point 1.

According to the series–parallel connections, the direct equivalent stiffness $k_{1,1}$ and the indirect equivalent stiffness ($k_{1,11}$, $k_{1,12}$, $k_{1,13}$, and $k_{1+1,14}$) in the equivalent model for the initial segment can be obtained as follows

$$k_{1,11} = \left\{\left[\left(k_{C,12}+k_{\mathrm{kj}}\right)\times(1-\delta_{12}) + k_{C,13}\times(1-\delta_{13})\right] + k_{C,1}\right\} \parallel k_{\mathrm{gg}} \quad (2)$$

$$k_{1,12} = \left(1-\frac{k_{1,11}}{k_{\mathrm{gg}}}\right)\delta_{12}k_{\mathrm{gd}} \quad (3)$$

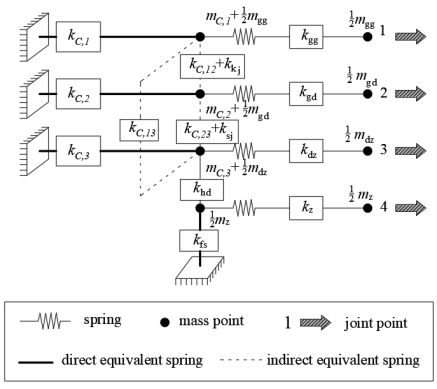

(a) Original FE model

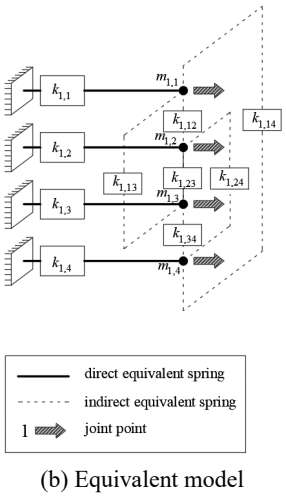

(b) Equivalent model

Fig. 2 Initial segment

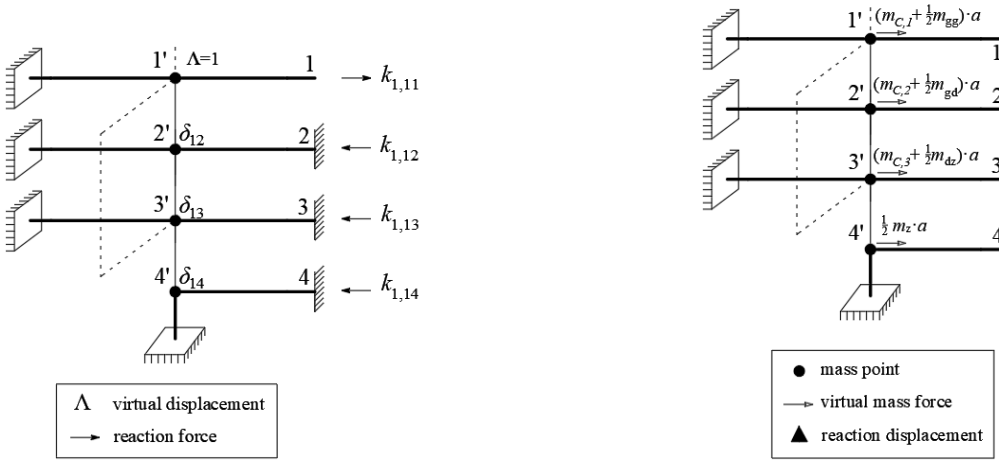

(a) Equivalent stiffness (b) Equivalent mass

Fig. 3 Virtual displacement/force applied to point 1

$$k_{1,13} = \left(1 - \frac{k_{1,11}}{k_{\mathrm{gg}}}\right)\delta_{13}k_{\mathrm{dz}} \tag{4}$$

$$k_{1,14} = \left(1 - \frac{k_{1,11}}{k_{\mathrm{gg}}}\right)\delta_{14}k_{z} \tag{5}$$

$$k_{1,1} = k_{1,11} - k_{1,12} - k_{1,13} - k_{1,14} \tag{6}$$

where ‖ denotes the series connection operation.

Similarly, the indirect equivalent stiffness related to points 2, 3 and 4, denoted as $k_{1,22}$, $k_{1,33}$, $k_{i+1,44}$, $k_{1,23}$, $k_{1,24}$, and $k_{1,34}$ can be obtained, and the direct equivalent stiffness related to Points 2, 3, and 4, denoted as $k_{1,2}$, $k_{1,3}$, and $k_{1,4}$, can be expressed as follows

$$k_{1,2} = k_{1,22} - k_{1,12} - k_{1,23} - k_{1,24} \tag{7}$$

$$k_{1,3} = k_{1,33} - k_{1,13} - k_{1,23} - k_{1,34} \tag{8}$$

$$k_{1,4} = k_{1,44} - k_{1,14} - k_{1,24} - k_{1,34} \tag{9}$$

To determine the equivalent mass at point 1, consolidation is conducted on points 2 and 3, and the virtual longitudinal unit acceleration a = 1 was applied to all mass points (Fig. 3(b)). The displacements on point 1 initiated by the mass force on points 1, 1', 2', 3' and 4' ($u_{1,11}$, $u_{1,11'}$, $u_{1,12'}$, $u_{1,13'}$, and $u_{1,14'}$) can be obtained. Then, the equivalent mass $m_{1,1}$ can be obtained using the superimposition method

$$m_{1,1} = \frac{k_{1,11}\left(u_{1,11} + u_{1,11'} + u_{1,12'} + u_{1,13'} + u_{1,14'}\right)}{a} \tag{10}$$

Similarly, the equivalent masses $m_{1,2}$, $m_{1,3}$, and $m_{1,4}$ can be obtained

$$m_{1,2} = \frac{k_{1,22}\left(u_{1,22} + u_{1,21'} + u_{1,22'} + u_{1,23'}\right)}{a} \tag{11}$$

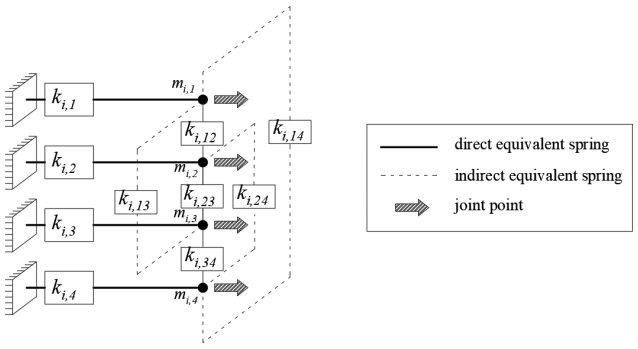

Fig. 4 The equivalent model for i^{th} segment

$$m_{1,3} = \frac{k_{1,33}\left(u_{1,33} + u_{1,31'} + u_{1,32'} + u_{1,33'}\right)}{a} \tag{12}$$

Then adjust the equivalent mass according to the first natural frequency.

2.2 Equivalence of general segments

According to an equivalent method, which is similar to the above method for the initial segment, the i^{th} segment and its preceding segment are equivalent to the equivalent model and called the equivalent model for the i^{th} segment (Fig. 4). By connecting the equivalent model for the i^{th} segment with the next segment, an equivalent model for the i+1$^{\mathrm{th}}$ segment can be established using the same method (Fig. 5).

Solving for the equivalent stiffness related to point 1 ($k_{i+1,1}$, $k_{i+1,12}$, $k_{i+1,13}$, and $k_{i+1,14}$), the equivalent mass related to point 1 ($m_{i+1,1}$) is taken as an example.

In solving for the equivalent stiffness, points 2, 3, and 4 were consolidated, and a unit displacement was applied to point 1'. By considering the series/parallel connection relationships of springs and the longitudinal force balance on points 2 and 3, the following equation can be obtained

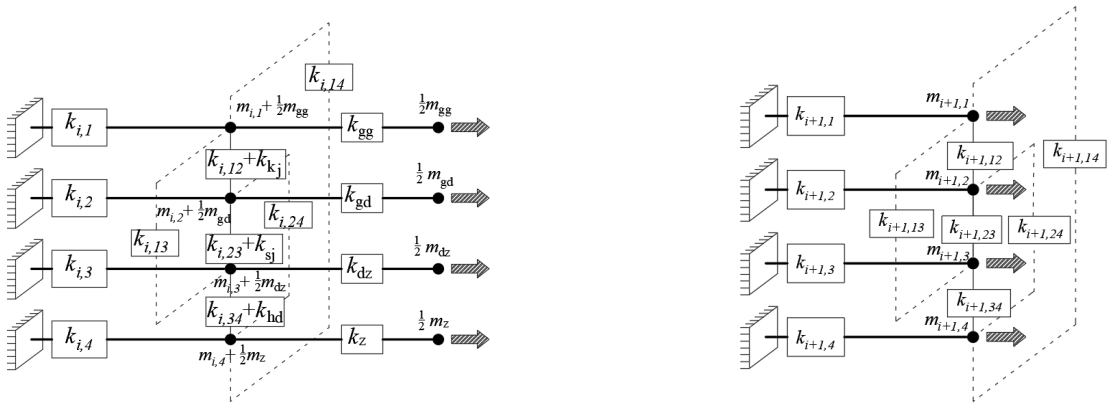

(a) Original FE model (b) Equivalent model

Fig. 5 The i+1[th] segment

$$\begin{pmatrix} k_{i,2}+k_{\mathrm{gd}}+k_{i,12}+k_{\mathrm{kj}} \\ +k_{i,23}+k_{\mathrm{sj}}+k_{i,24} & -k_{i,23}-k_{\mathrm{sj}} & -k_{i,24} \\ -k_{i,23}-k_{\mathrm{sj}} & k_{i,3}+k_{\mathrm{dz}}+k_{i,13}+k_{i,23} \\ & +k_{\mathrm{sj}}+k_{i,34}+k_{\mathrm{hd}} & -k_{i,34}-k_{\mathrm{hd}} \\ -k_{i,14} & -k_{i,24} & k_{i,4}+k_z+k_{i,14} \\ & & +k_{i,24}+k_{i,34}+k_{\mathrm{hd}} \end{pmatrix} \begin{pmatrix} 1-\delta_{12} \\ 1-\delta_{13} \\ 1-\delta_{14} \end{pmatrix} = \begin{pmatrix} k_{i,2}+k_{\mathrm{gd}} \\ k_{i,3}+k_{\mathrm{dz}} \\ k_{i,4}+k_z \end{pmatrix} \tag{13}$$

where $\delta_{12}, \delta_{13}, \delta_{14}$ denote the joint displacement at points 2', 3', and 4' caused by the unit displacement of point 1.

Then the direct equivalent stiffness $k_{i+1,1}$ and the indirect equivalent stiffness $k_{i+1,11}$, $k_{i+1,12}$, $k_{i+1,13}$, and $k_{i+1,14}$ in the equivalent model for the i+1[th] segment can be obtained as follows

$$\begin{aligned} k_{i+1,11} = \{[&(k_{i,12}+k_{\mathrm{kj}})\times(1-\delta_{12}) \\ &+k_{i,13}\times(1-\delta_{13}) \\ &+k_{i,14}\times(1-\delta_{14})]+k_{i,1}\} \parallel k_{\mathrm{gg}} \end{aligned} \tag{14}$$

$$k_{i+1,12} = \left(1-\frac{k_{i+1,11}}{k_{\mathrm{gg}}}\right)\delta_{12}k_{\mathrm{gd}} \tag{15}$$

$$k_{i+1,13} = \left(1-\frac{k_{i+1,11}}{k_{\mathrm{gg}}}\right)\delta_{13}k_{\mathrm{dz}} \tag{16}$$

$$k_{i+1,14} = \left(1-\frac{k_{i+1,11}}{k_{\mathrm{gg}}}\right)\delta_{14}k_z \tag{17}$$

$$k_{i+1,1} = k_{i+1,11}-k_{i+1,12}-k_{i+1,13}-k_{i+1,14} \tag{18}$$

To determine the equivalent mass of point 1, consolidation is conducted on points 2, 3, and 4, and a unit acceleration a = 1 was applied to all mass points. In consideration of the indirect equivalent stiffness, the displacements of point 1 caused by the mass forces at points 1, 1', 2', 3', and 4' can be obtained and expressed as $u_{i+1,11}$, $u_{i+1,11'}$, $u_{i+1,12'}$, $u_{i+1,13'}$, and $u_{i+1,14'}$, respectively. The equivalent mass $m_{i+1,1}$ can be obtained using the superposition method

Then adjust the equivalent mass according to the first natural frequency. Similarly, the indirect equivalent stiffness ($k_{i+1,22}$, $k_{i+1,33}$, $k_{i+1,44}$, $k_{i+1,23}$, $k_{i+1,24}$, and $k_{i+1,34}$), the direction equivalent stiffness ($k_{i+1,2}$, $k_{i+1,3}$, and $k_{i+1,4}$), and the equivalent masses ($m_{i+1,2}$, $m_{i+1,3}$, and $m_{i+1,4}$) related to points 2, 3, and 4 in the equivalent model for i+1[th] segment can be obtained. Subsequently, by connecting the equivalent model with the subsequent segment and solving for the equivalent stiffness and equivalent masses in the equivalent model for subsequent segment, the final equivalent stiffnesses ($K_{N,1}$, $K_{N,2}$, $K_{N,3}$, $K_{N,4}$, $K_{N,12}$, $K_{N,13}$, $K_{N,14}$, $K_{N,23}$, $K_{N,24}$, and $K_{N,34}$) and final equivalent masses ($M_{N,1}$, $M_{N,2}$, $M_{N,3}$, and $M_{N,4}$) of the entire adjoining-bridge structure can be obtained. The entire adjoining structure was converted

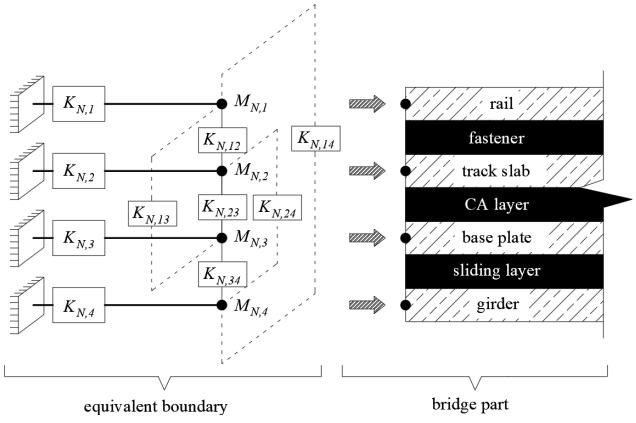

Fig. 6 Converting the adjoining-bridge structure to an equivalent boundary

$$m_{i+1,1} = \frac{k_{i+1,11}\left(u_{i+1,11}+u_{i+1,11'}+u_{i+1,12'}+u_{i+1,13'}+u_{i+1,14'}\right)}{a} \tag{19}$$

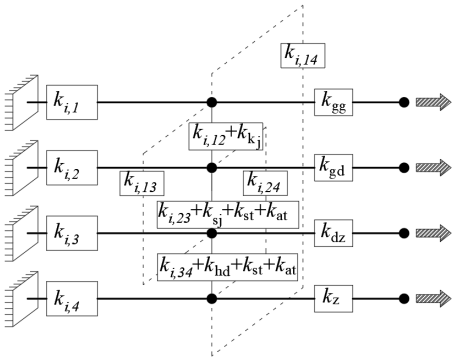

Fig. 7 The segments with special interlayer components

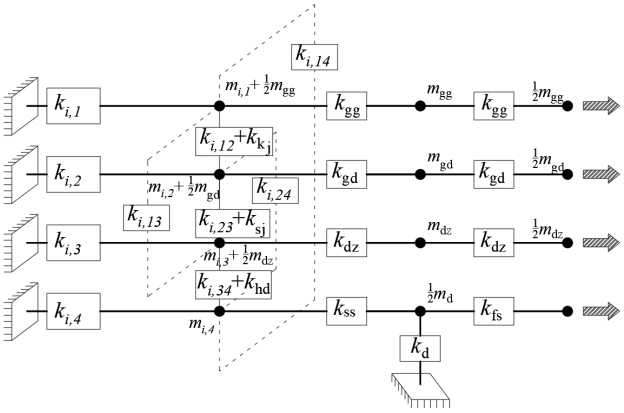

Fig. 8 The segment at the gap between girders

into the equivalent boundary system of the target structure (Fig. 6). The subscript N denotes the span number of the adjoining structure.

2.3 Equivalence of special segments

The equivalence of some special segments is not quite the same as the above equivalence process, which includes the segments containing special interlayer components and the segments of subgrade section. For these segments, the equivalent stiffness and equivalent mass should be adjusted correspondingly.

(1) For segments with special interlayer components, including shear teeth (fixed to the girder on the top of the fixed bearing), shear rebar, and lateral block, the special interlayer components are in parallel with ordinary interlayer components, including the sliding layer and CA layer (Fig. 7). The stiffness of sliding layer and CA layer after the adjustment can be calculated as follows

$$k'_{\mathrm{hd}} = k_{\mathrm{hd}} + k_{\mathrm{st}} + k_{\mathrm{at}} \tag{20}$$

$$k'_{\mathrm{sj}} = k_{\mathrm{sj}} + k_{\mathrm{ht}} + k_{\mathrm{at}} \tag{21}$$

where k_{st}, k_{ht}, and k_{at} denote the longitudinal stiffness of shear teeth, shear rebar, and lateral block, respectively.

(2) For the segment of adjoining subgrade structure, the spring and mass of girder should be removed; the bridge pier and bearing should be regarded as a rigid body. Moreover, the stiffness of subgrade k_{dj} is used to replace the stiffness of sliding layer

$$k'_z + k'_d \parallel k'_{\mathrm{fs}} = \infty \tag{22}$$

$$k'_{\mathrm{hd}} = k_{\mathrm{dj}} \tag{23}$$

(3) If the foundation does not meet the rigid connection between the pier bottom and the ground, the stiffness of pier is adjusted to

$$k'_d = k_d \parallel k_p \tag{24}$$

where k_{p} denotes the stiffness of the pier bottom.

(4) For the segments at the gap between girders, k_{ss}, k_{d} and k_{fs} connected with $k_{i,4}$ in place of k_z are as shown in Fig. 8 where k_{d} denotes the unit longitudinal stiffness of the pier.

3. Case study on coupling span number

Due to the longitudinal constraint of the track system, the target structure will be affected by other spans within a certain number, called coupling span number. Determining the coupling span number before applying the model can greatly improve the calculation efficiency and ensure accurate results. In order to examine the coupling span number of the target structure, large quantities of equivalent FE models of HSRSBs with different span numbers were established using ANSYS software.

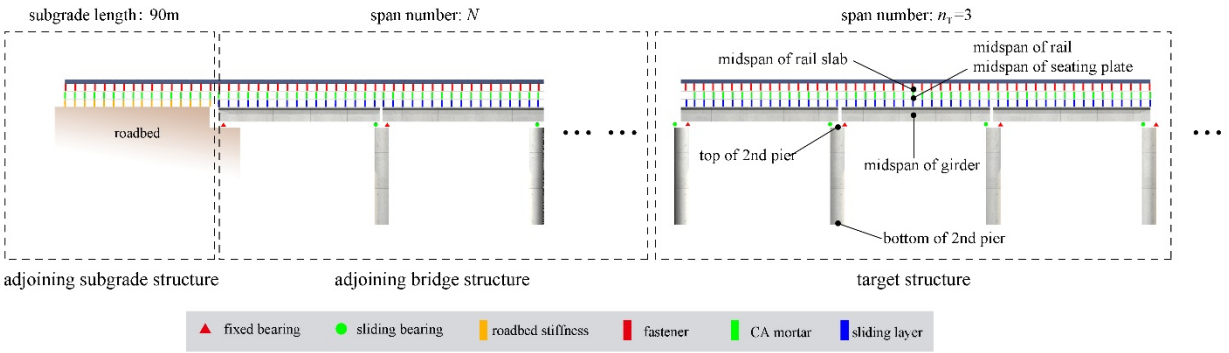

Fig. 9 The adjoining structure in Side A of the target structure

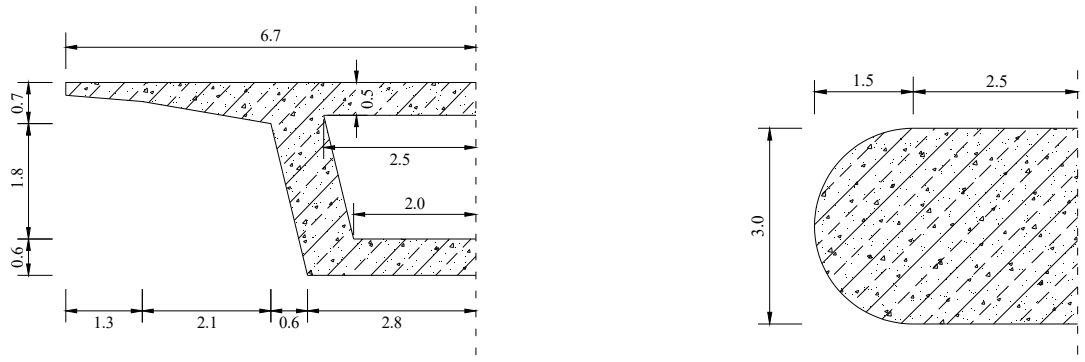

(a) Girder (b) Pier

Fig. 10 Cross-section (unit: m)

3.1 Bridge model

Previous studies have shown that the displacement response of the middle span is usually the largest compared with other spans in the HSRSB (Yan *et al*. 2017, Zhang *et al*. 2020). Therefore, the middle three-span bridge was selected as the target structure, and the span number of the target structure was denoted as $n_T = 3$. The two sides of the target structure are connected with a *N*-spans adjoining-bridge, and the total span number in the HSRSB is $n = 2 \times N + n_T$ (Fig. 9). The side near the fixed bearing of target structure is assumed to be Side A, whereas the side near the sliding bearing is assumed to be Side B. Based on previous research, a 90 m subgrade section length is reasonable; therefore, the total equivalent stiffness and equivalent mass of the adjoining-subgrade structure will take the 90m subgrade length. And the equivalent subgrade characteristics are followed: $k_{C,1}$, $k_{C,2}$, $k_{C,3}$, $k_{C,12}$, $k_{C,13}$, and $k_{C,23}$ are 1.654e5 kN/m, 1.076e6 kN/m, 1.365e6, kN/m 2.034e5 kN/m, 5.270e4 kN/m, and 1.713e6 kN/m, respectively; $m_{C,1}$, $m_{C,2}$, and $m_{C,3}$ are 3.857 kN/g, 24.252 kN/g, and 23.821 kN/g, respectively. $k_{C,1}$ $k_{C,2}$ and $k_{C,3}$ represent the direct equivalent stiffness of the equivalent subgrade structure, and $k_{C,12}$, $k_{C,23}$, and $k_{C,13}$ represent the indirect equivalent stiffness of the equivalent subgrade structure. $m_{C,1}$, $m_{C,2}$, $m_{C,3}$ are the equivalent masses of the equivalent subgrade structure.

The main components were simulated using beam elements, including girders, piers, base slabs, track slabs, and rails. Girders are composed of typical 32 m double-line standard simply-supported beams and C30 concrete. Piers are composed of C40 concrete. Base slabs, track slabs, and rails use standard CRTSII ballastless track materials. The girder cross-section and pier cross-section are shown in Fig. 10. In order to explore the impact of component parameters on seismic response of the target structure, different pier heights (10 m, 20 m, and 30 m) and pier bottom stiffnesses (H_1 and H_2) were analyzed (Table 1). The length of each girder element is 0.645 m, and the number of elements of each pier is 20.

Fasteners, CA mortar, sliding layers, shear teeth, shear rebar, lateral blocks, and bearings were used to connect the main components. Spring elements were used to simulate interlayer components; the mass of the interlayer components was not considered and interlayer components were composed of linear elastic materials. The roadbed is assumed to be a rigid body. All interlayer connecting components are listed in Table 2 for an element length of 0.645 m.

Table 1 Two kind stiffness of the pier bottom (unit: kN, m)

	Direction					
	X	*Y*	*Z*	ROT*X*	ROT*Y*	ROT*Z*
H_1	2.97e7	3.28e7	6.67e7	1.49e9	7.61e8	1.0e12
H_2	2.20e6	2.34e6	1.46e7	3.39e8	1.78e8	1.0e12

Table 2 Stiffness of interlayer components (unit: kN/m)

Component	Direction	
	Longitudinal	Vertical
Fastener	4.33E+03	1.38E+04
CA mortar layer	9.00E+04	2.00E+09
Sliding layer	1.20E+04	1.38E+09
Shear rebar	2.40E+06	2.00E+09
Shear teeth	1.00E+09	1.39E+09
Lateral block	1.20E+04	1.38E+09
Fixed bearing	2.58E+06	1.00E+07
Sliding bearing	2.58E+04	1.00E+07

To preliminarily study the target structure coupling span number under earthquake conditions, an earthquake record with a peak acceleration of 0.2 g and a characteristic period (Tg) of 0.35 s was selected for seismic analysis. The acceleration time history and the acceleration spectrum are shown in Fig. 11. Rayleigh damping was applied to all structural components with a damping ratio of 3% associated to 1st mode and 2nd mode.

Fig. 12 shows the simplification efficiency of equivalent FE model with different span number, reflecting reduction of elements by equivalent FE model. The simplification efficiency is defined as $\zeta_s = (e_{fb} - e_{eq})/e_{fb}$ where e_{fb} and e_{eq} denote the element number of the original FE model and the equivalent FE model respectively. The simplification efficiency of the equivalent FE model was over 75%, and

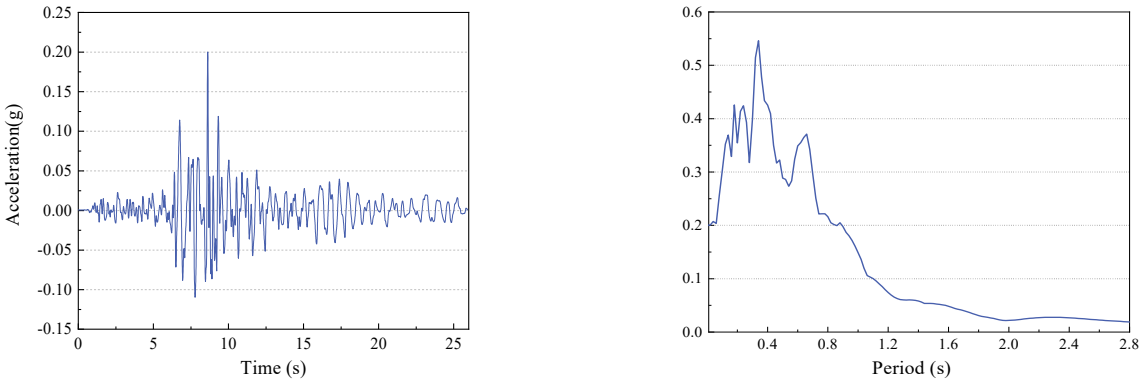

(a) Acceleration time (b) Acceleration spectrum

Fig. 11 Earthquake record

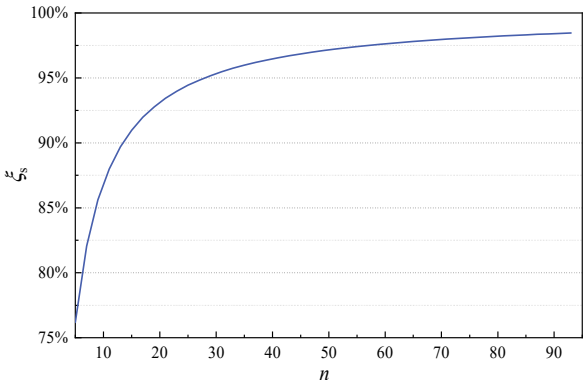

Fig. 12 The simplification efficiency of equivalent FE model with different span number

increased with the increasing span number. The simplification efficiency could reach 98.4% as the span number increased to 93. It indicates that the equivalent FE model can greatly reduce the complexity of the original FE model.

3.2 Equivalent boundary characteristic sensitivity

To describe the variation in equivalent stiffness and equivalent mass with increasing adjoining-bridge span number (N) and explore association between the equivalent boundary characteristics and the seismic response with varying adjoining-bridge span number (N), the sensitivity of equivalent stiffness K with respect to N is defined as follows

$$G(N,K)=\left(\frac{|K_{N+1}-K_N|}{K_{N+1}-K_N}\right)\left[1-exp\left(-\left|\frac{K_{N+1}}{K_N}-1\right|\right)\right] \quad (25)$$

The equivalent mass M sensitivity with respect to N is defined as follows

$$G(N,M)=\left(\frac{|M_{N+1}-M_N|}{M_{N+1}-M_N}\right)\left[1-exp\left(-\left|\frac{M_{N+1}}{M_N}-1\right|\right)\right] \quad (26)$$

where K_N and M_N are the equivalent stiffness and the equivalent stiffness when the adjoining-bridge span number is N.

The higher the absolute value of sensitivity G, the greater is the expected variation in K or M (e.g., K or M becomes more unstable with respect to N). In contrast, G approaching zero indicates the stable condition.

The sensitivity of the equivalent boundary characteristic of side A under the H_1 condition is given in Figs. 13-15. When the number of adjoining bridge spans (N) is small, the absolute values of equivalent stiffness sensitivity and equivalent mass sensitivity were both higher. As N increased, the sensitivities approached 0, indicating that the

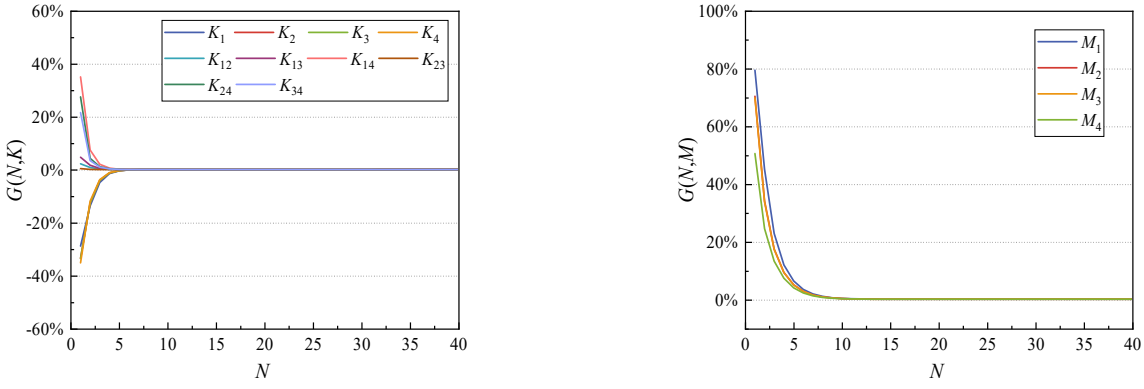

(a) Equivalent stiffness (b) Equivalent mass

Fig. 13 Sensitivity (in H_1 and pier heights of 10 m) of A side

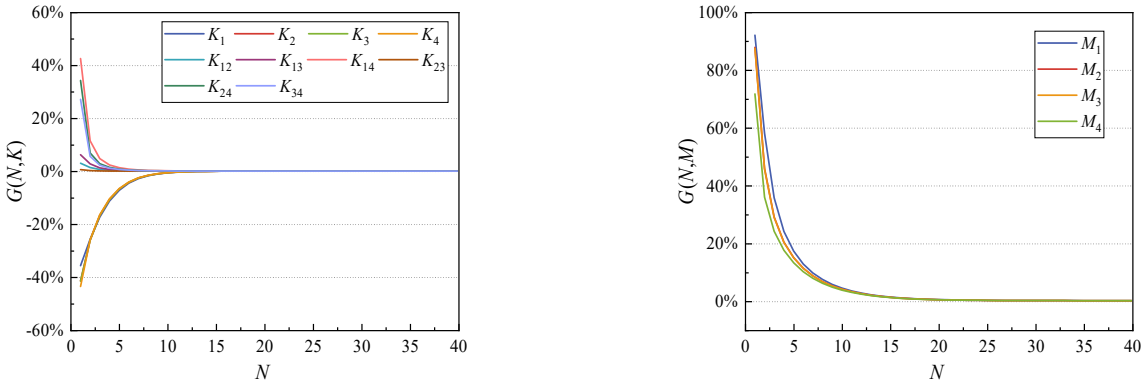

(a) Equivalent stiffness (b) Equivalent mass

Fig. 14 Sensitivity (in H_1 and pier heights of 20 m) of A side

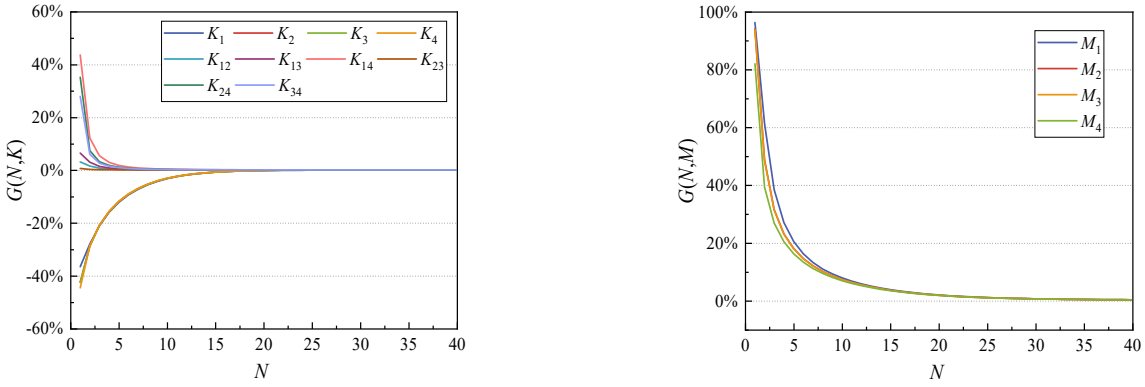

(a) Equivalent stiffness (b) Equivalent mass

Fig. 15 Sensitivity (in H_1 and pier heights of 30 m) of A side

equivalent stiffness and equivalent mass eventually approach stable values. Pier height also affects the sensitivity and the number of stable spans.

In order to determine the number of possible stable spans, the determination index for the critical equivalent stiffness sensitivity point is defined as

$$\begin{cases} |\varepsilon(N,K)| = |G(N+1,K) - G(N,K)| < \delta \\ |G(N,K)| < \delta \\ N \geq \widetilde{N} \end{cases} \tag{27}$$

The determination index for the critical equivalent mass sensitivity is defined as

$$\begin{cases} |\varepsilon(N,M)| = |G(N+1,M) - G(N,M)| < \delta \\ |G(N,M)| < \delta \\ N \geq \widetilde{N} \end{cases} \tag{28}$$

where $\varepsilon(N, K)$ and $\varepsilon(N, M)$ denote sensitivity variations in equivalent stiffness and equivalent mass, respectively. δ denotes the allowable values, and $\widetilde{N}$ denotes the minimum number of adjoining-bridge spans that meets the critical point determination condition.

When N on both sides reaches $\widetilde{N}$, if $|\varepsilon(N, K)|$ and $G(N, K)|$ are both always less than δ, under the current δ standard, the critical equivalent stiffness sensitivity point is $\widetilde{N}$. Likewise, if $|\varepsilon(N, M)|$ and $|G(N, M)|$ are both always less than δ, under the current δ standard, the critical equivalent mass sensitivity point is $\widetilde{N}$. In particular, when the equivalent stiffness and equivalent mass meet the determination condition of the critical point for the same span number, under the current δ standard, the critical sensitivities point for the equivalent boundary characteristics is $\widetilde{N}$.

When 0.1% was selected as the allowable value, critical sensitivities point for the equivalent boundary characteristics were obtained for different pier heights and pier bottom stiffnesses (Table 3).

It can be seen that: (1) the equivalent mass sensitivity critical points were larger than that of equivalent stiffness, indicating that the change in equivalent mass is more unstable than that of equivalent stiffness. (2) The sensitivity critical points on side A were slightly larger than on side B, indicating that the order of component layout in the adjoining-bridge has an influence on critical point sensitivity. (3) For the pier bottom stiffness H_1, the equivalent boundary characteristic critical points for a pier height of 10 m, 20 m, and 30 m were respectively 9-span, 15-span, and 25-span, and the corresponding total span number for the whole bridge were 21-span, 33-span, and 53-span. For the pier bottom stiffness H_2, the equivalent boundary characteristic critical points for a pier height of 10 m, 20 m, and 30 m were respectively 12-span, 22-span, and 27-span, and the corresponding total span number of the

whole bridge were 27-span, 47-span, and 57-span.

Table 3 Critical sensitivities point for the equivalent boundary characteristics

	Pier height	Side	Critical sensitivities points $\widetilde{N}$		
			K	M	Equivalent boundary characteristics
H_1	10 m	A	6	9	9
		B	4	9	
	20 m	A	9	15	15
		B	9	14	
	30 m	A	16	25	25
		B	15	25	
H_2	10 m	A	7	12	12
		B	6	11	
	20 m	A	12	22	22
		B	11	20	
	30 m	A	18	27	27
		B	17	26	

3.3 Dynamic characteristics of the target structure

3.3.1 Analysis of natural vibration

The acceleration magnification factors corresponding to the first natural period of the equivalent FE models with varying total spans (n = 5~93) under different pier heights and pier bottom stiffnesses are shown in Figs. 16-18. The degree of color depth represents the distribution density of the calculation examples for the corresponding first natural period. The deeper the color is, the more calculation examples are distributed near the period. The period corresponding to the maximum acceleration magnification factor in the distribution is called maximum magnification period (P_{MM}), and the span number in the HSRSB closest to P_{MM} is called the span number with maximum magnification (N_{NMM}).

It can be seen from Figs. 16-18 that: (1) when n is low, the first natural period of HSRSBs increased greatly with increasing n; however, as n increases further, the distribution density gradually increases, that is, the effect of n on the first natural period was no longer significant. (2) The pier height had a significant influence on the first natural period of HSRSBs. The higher the pier, the larger the first natural period, and under different pier heights, there were significant variations in N_{NMM}. (3) Pier bottom

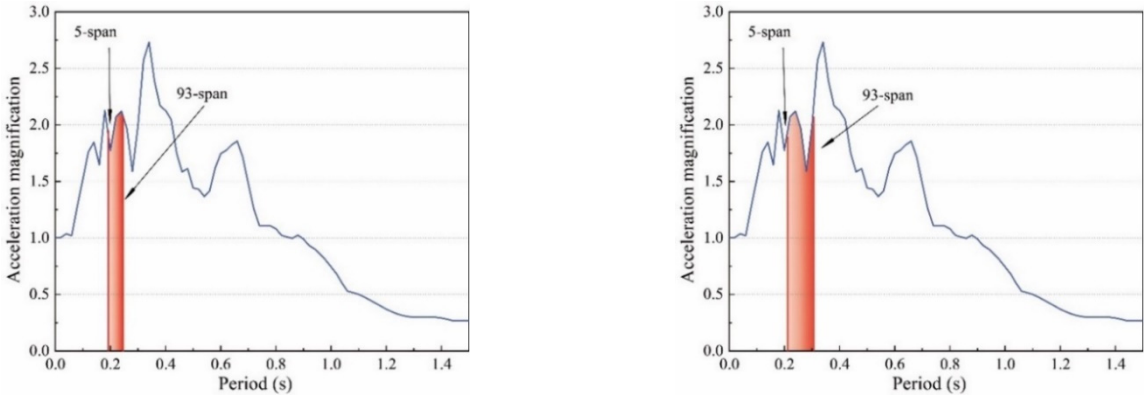

(a) H_1 (b) H_2

Fig. 16 The acceleration magnification factors corresponding to the first natural period in 10 m pier height

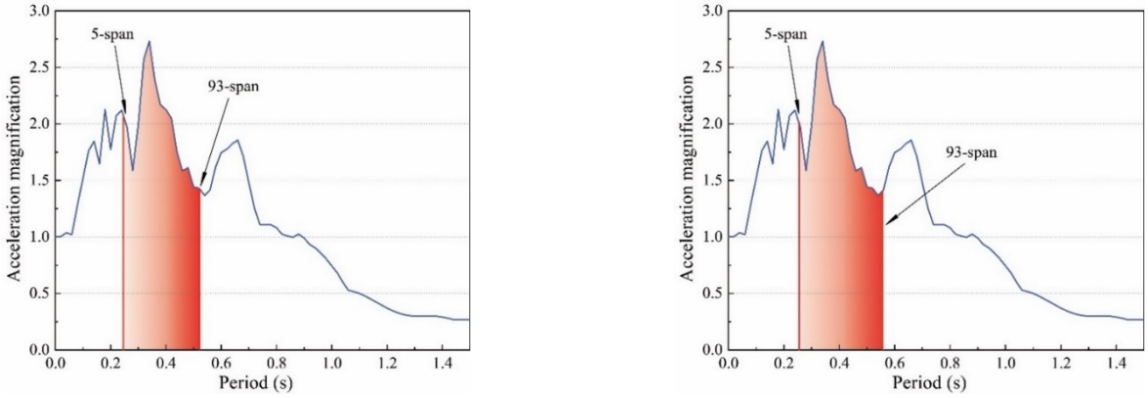

(a) H_1 (b) H_2

Fig. 17 The acceleration magnification factors corresponding to the first natural period in 20 m pier height

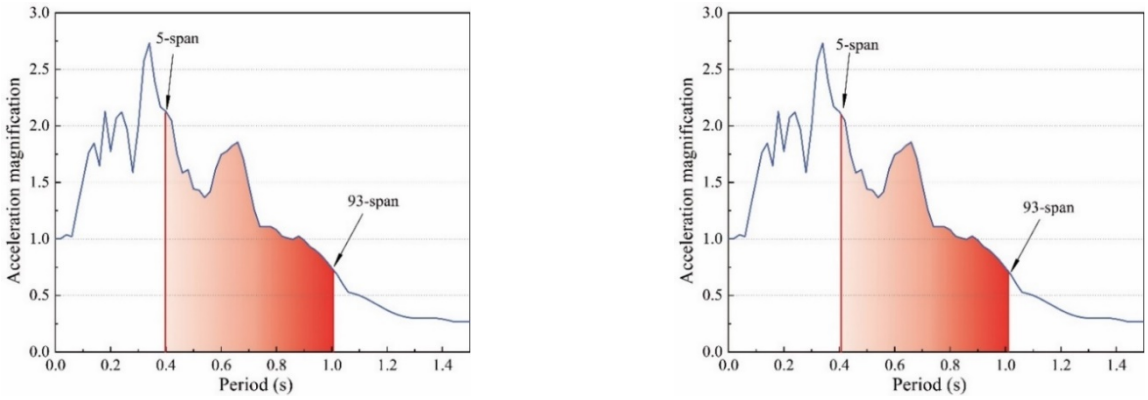

(a) H_1 (b) H_2

Fig. 18 The acceleration magnification factors corresponding to the first natural period in 30 m pier height

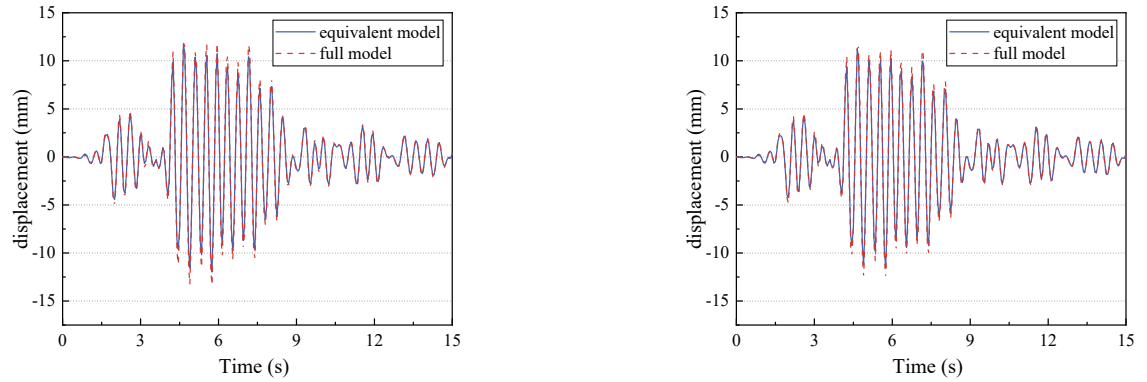

(a) TR_1 (b) TR_2

Fig. 19 Comparison of results of 15-span HSRSB obtained by equivalent model and full model (a) TR_1; (b) TR_2

stiffness had no significant effect on the first natural period of HSRSBs. The first natural period for H_2 was only slightly larger than for H_1.

3.3.2 Analysis of peak seismic response

To validate the rationality of equivalent model, the longitudinal seismic responses of 15-span HSRSB obtained by equivalent model and full finite element model were compared. Dynamic analysis was carried out to obtain the seismic responses. The results obtained by equivalent model for comparison included longitudinal displacement of middle rail (TR_1), longitudinal displacement of the 2nd pier top (TR_2). The results of the equivalent model very close to those of full model in the time history curves as shown in Fig. 19, indicating that the equivalent model has acceptable calculation accuracy.

The calculation results of peak seismic response for target structures with varying n, pier heights (10 m, 20 m, and 30 m), and pier bottom stiffness (H_1 and H_2) are shown in Figs. 20-23, including peak rail longitudinal displacement (D_r), peak longitudinal displacement of the 2nd pier (D_2), peak shear of the 2nd pier bottom (F_2), and peak

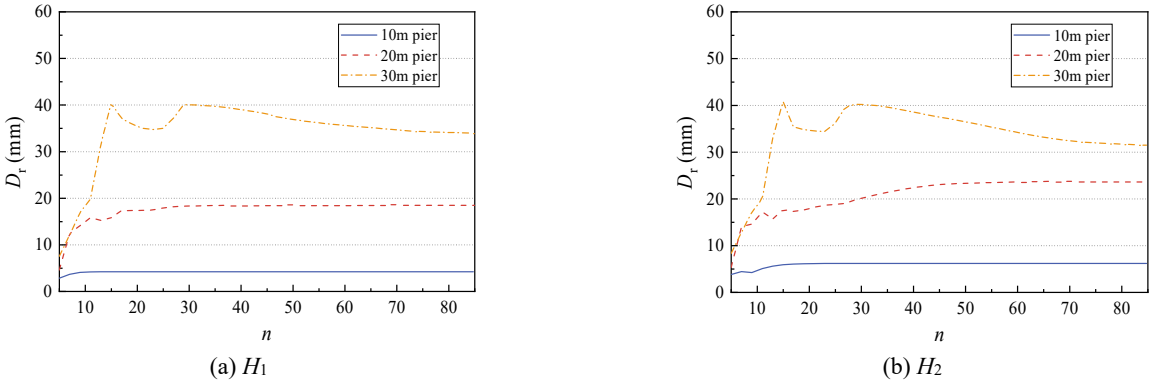

(a) H_1 (b) H_2

Fig. 20 Peak displacement of rail D_r

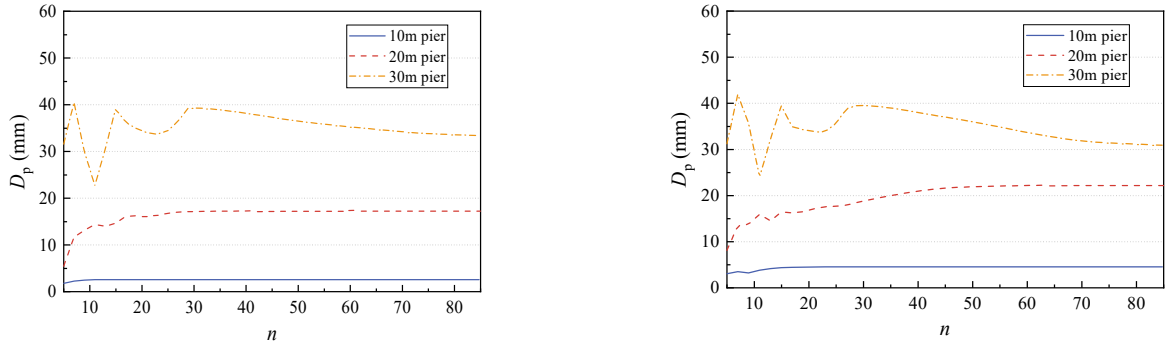

(a) H_1 (b) H_2

Fig. 21 Peak displacement of the 2nd pier D_2

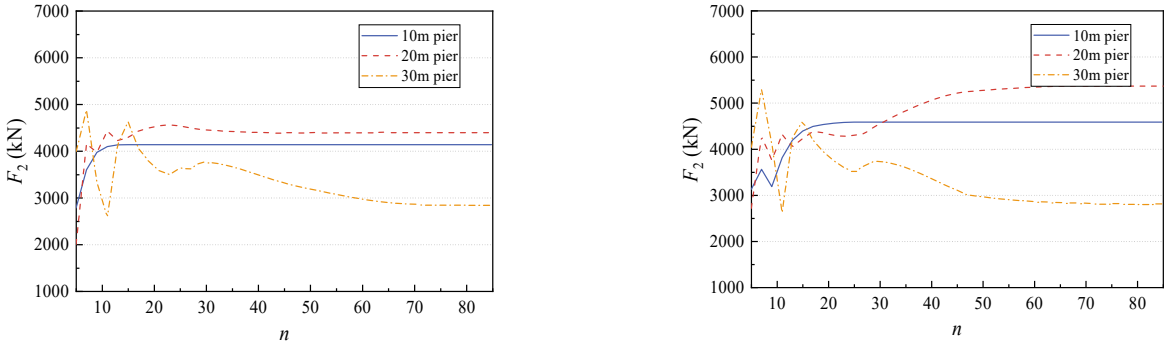

(a) H_1 (b) H_2

Fig. 22 Peak shear of the 2nd pier bottom F_2

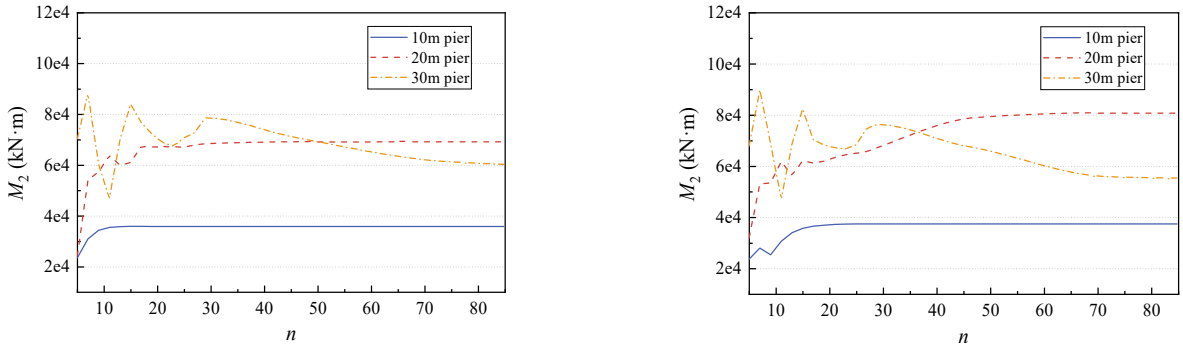

(a) H_1 (b) H_2

Fig. 23 Peak bending moment of the 2nd pier bottom M_2

bending moment of the 2nd pier bottom (M_2). Dynamic analysis was carried out to obtain these seismic responses.

It can be seen from Figs. 20-23 that: (1) With increasing n, the peak seismic response of the target structure changed sharply at first and then stabilized. The target structure had negative span number of the seismic response (N_{NS}) and stable span number of the seismic response (N_{SSE}). The maximum peak seismic response appeared under N_{NS}, which was significantly higher than peak seismic responses under the nearby spans. When n reached N_{SSE}, the peak seismic response of the target structure no longer changed with increasing n. (2) When n was low, high pier and small pier bottom stiffness amplified the seismic responses of the target structure. (3) There is a correlation between N_{NS} in the seismic response of the target structure and N_{NMM} in the natural vibration; hence, N_{NS} can be roughly found by calculating N_{NMM}. (4) For identical pier heights and pier bottom stiffnesses, N_{NS} and N_{SSE} for different seismic responses (i.e., D_r, D_2, F_2, and M_2) are basically the same.

3.4 Method for determining the coupling span number

In order to examine the coupling span number of the target structure, the peak seismic response sensitivity of the target structure with respect to n is defined as follows

$$G(n,R)=\left(\frac{|R_{n+1}-R_n|}{R_{n+1}-R_n}\right)\left[1-exp\left(-\left|\frac{R_{n+1}}{R_n}-1\right|\right)\right] \quad (29)$$

And the determination index for critical point of peak seismic response sensitivity is defined as

$$\begin{cases}|\varepsilon(n,R)|=|G(n+2,R)-G(n,R)|<\delta\\ |G(n,R)|<\delta\\ n\geq\tilde{n}\end{cases} \quad (30)$$

where R_n denotes the peak seismic response at any part of the target structure when total span number in the HSRSB is n, $\varepsilon(n, R)$ denotes the variation in peak seismic response sensitivity, δ denotes the allowable value, and $\tilde{n}$ is the minimum span number in the HSRSB that meets the critical point determination condition. When n reaches $\tilde{n}$, if $|G(n, R)|$ and $|\varepsilon(n, R)|$ are both always less than δ, under the current δ standard, the critical sensitivity point for the peak seismic response is $\tilde{n}$. In particular, when the seismic response peaks in all parts of the target structure meet the determination condition for the critical point at the same span number, $\tilde{n}$ is the coupling span number of the target structure under the standard of δ.

The sensitivity for peak seismic response of the target structure with respect to n under different pier heights (10 m, 20 m, and 30 m) and pier bottom stiffness (H_1 and H_2)

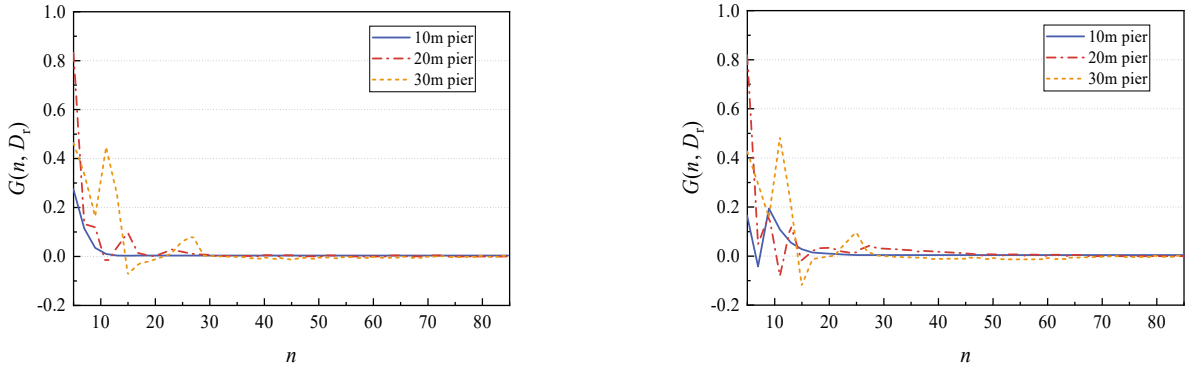

(a) H_1 (b) H_2

Fig. 24 Sensitivity for peak displacement of rail

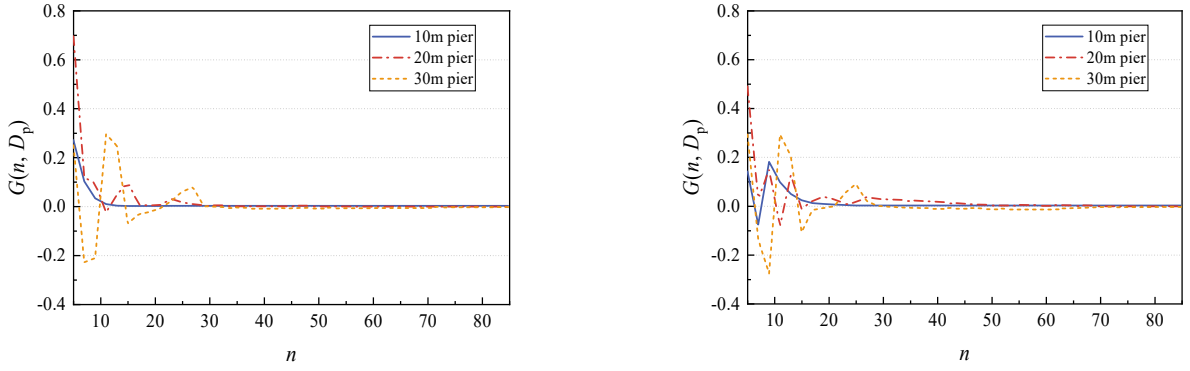

(a) H_1 (b) H_2

Fig. 25 Sensitivity for peak displacement of the 2nd pier bottom

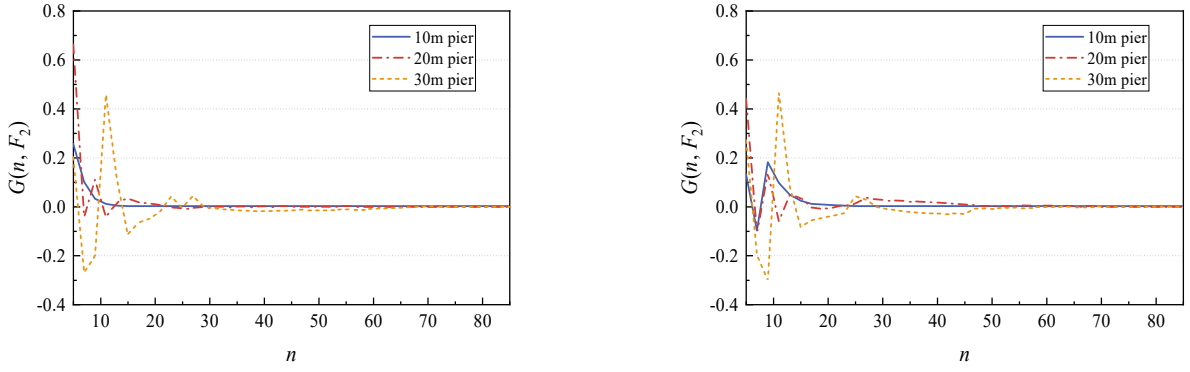

(a) H_1 (b) H_2

Fig. 26 Sensitivity for peak shear of the 2nd pier bottom

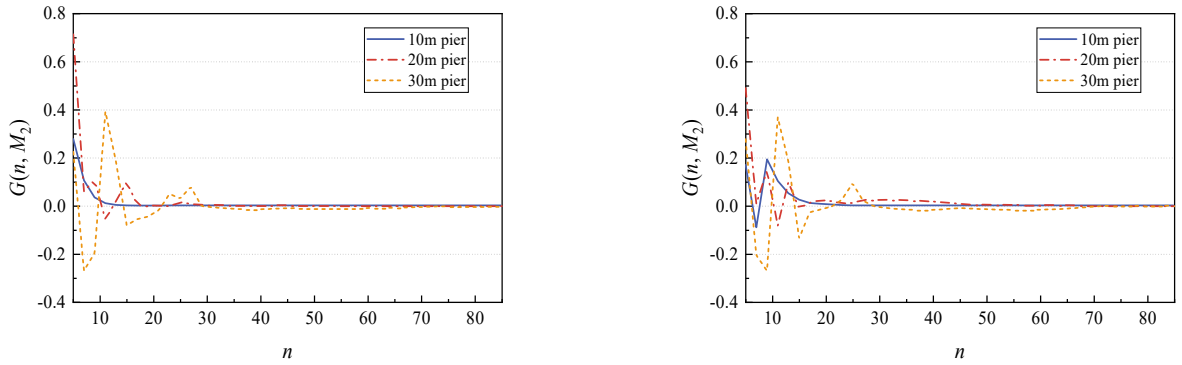

(a) H_1 (b) H_2

Fig. 27 Sensitivity for peak bending moment of the 2nd pier bottom

Table 4 Critical sensitivity point and coupling span number

	Pier height	Critical sensitivity point for peak seismic response							Coupling span number
		D_r	D_t	D_p	D_g	D_2	F_2	M_2	
H_1	10 m	15	17	17	15	15	15	19	19
	20 m	29	29	29	29	29	25	29	29
	30 m	47	51	49	49	53	51	49	53
H_2	10 m	25	25	25	23	25	23	23	25
	20 m	45	47	47	45	47	47	47	47
	30 m	55	53	55	57	55	53	59	59

are shown in Figs. 24-27. When n is small, sensitivities changed significantly with increasing n, but as n increases further, sensitivities begin to moderate and eventually approach 0. The higher the pier height and the smaller the pier bottom stiffness, the larger the span number in the target structure needed to reach a stable seismic response sensitivity ($\tilde{n}$). For identical pier heights and pier bottom stiffness, $\tilde{n}$ for the seismic response at any part of the target structure was basically the same.

When 0.1% was considered as the allowable value, the critical sensitivity point can be obtained (Table 4), including peak rail displacement (D_r), peak track slab displacement (D_t), peak base slab displacement (D_p), peak girder displacement (D_g), peak displacement of the 2nd pier (D_2), peak shear of the 2nd pier bottom (F_2), and peak bending moment of the 2nd pier bottom (M_2). Pier height and pier bottom stiffness had significant influence on the coupling span number of the target structure. For a pier bottom stiffness of H_1, the coupling span number of the target structure for pier heights of 10 m, 20 m, and 30 m were 19-span, 29-span, and 53-span, respectively. For a pier bottom stiffness of H_2, the coupling span number of target structure for pier heights of 10 m, 20 m, and 30 m were 25-span, 47-span and 59-span, respectively.

It can be seen that the coupling span number were approximately consistent with those for the sensitivity critical points for the equivalent boundary characteristics (section 4.2), indicating that the coupling span number of the target structure can be obtained by sensitivity analysis of the equivalent boundary characteristics. Due to having high computational efficiency, sensitivity analysis of

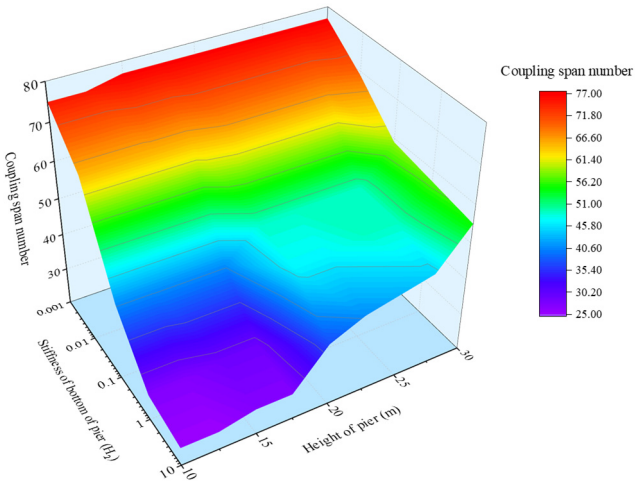

Fig. 28 Coupling span number in different condition

equivalent boundary characteristics is one of the most suitable methods for quickly determining the coupling span number of target structure and is called the Sensitivity for Equivalent Boundary Characteristic Method (SEBCM). The coupling span number calculation formula can be expressed as

$$\tilde{n} = 2 \times \tilde{N} + n_T \tag{31}$$

where $\tilde{n}$ denotes the coupling span number, $\tilde{N}$ denotes the critical point of sensitivities for equivalent boundary characteristics, and n_T denotes the span number of the target structure.

The coupling span number of the target structure under different pier heights (10 m~30 m) and pier bottom stiffness (0.001 H_2~10 H_2) are calculated using the SEBCM (Fig. 28). The higher the pier height and the smaller the pier bottom stiffness, the larger the coupling span number. The lower the pier height, the more significant the influence of pier bottom stiffness on coupling span number. The higher the pier bottom stiffness, the more significant the influence of pier height on coupling span number.

4. Conclusions

Considering the longitudinal effect of the track system, accurate and efficient equivalent FE models for HSRSBs were established. The natural vibration characteristics and seismic response of a large number of equivalent linear elastic FE models for HSRSBs with different amounts of spans (5-span to 93-span), different pier heights and pier bottom stiffness were calculated. Though the proposed method is currently applicable to linear elastic FE model, it could be helpful for nonlinear analysis in the future. The following conclusions are obtained:

- The equivalent FE model can greatly reduce the overall complexity of the original FE model.
- Based on the correlation between N_{NS} in the seismic response of the target structure and N_{NMM} in the natural vibration, N_{NS} can be roughly found by calculating the N_{NMM} when designing the span number in a bridge.
- With increasing span number in the HSRSB, seismic response sensitivity tends to be stable. The higher the pier height and the smaller the pier bottom stiffness, the larger the span number is required to reach a stable sensitivity.
- The coupling span number of the target structure can be obtained by using the SEBCM, which avoids a large number of complex seismic response calculations and improves the research efficiency significantly.
- Pier height and the pier bottom stiffness significantly affect the coupling span number of the target structure. The higher the pier height and the smaller the pier bottom stiffness, the larger the coupling span number is.

Acknowledgments

The research described in this paper was financially supported by the National Natural Science Foundation of China (Grant Number U1934207 and 51778630) and the Innovation-driven Plan in Central South University (2020zzts159).

References

Feng, Y., Jiang, L., Zhou, W., Lai, Z. and Chai, X. (2019), "An analytical solution to the mapping relationship between bridge structures vertical deformation and rail deformation of high-speed railway", *Steel Compos. Struct., Int. J.*, **33**(2), 209-224. https://doi.org/10.12989/scs.2019.33.2.209

Gou, H., Yang, L., Leng, D., Bao, Y. and Pu, Q. (2018), "Effect of bridge lateral deformation on track geometry of high-speed railway", *Steel Compos. Struct., Int. J.*, **29**(2), 219-229. https://doi.org/10.12989/scs.2018.29.2.219

Iemura, H., Iwata, S. and Murata, K. (2004), *Shake table tests and numerical modeling of seismically isolated railway bridges*, Vancouver, B.C., Canada.

Jankowski, R., Wilde, K. and Fujino, Y. (1998), "Pounding of superstructure segments in isolated elevated bridge during earthquakes", *Earthq. Eng. Struct. D*, **27**(5), 487-502. https://doi.org/10.1002/(SICI)1096-9845(199805)27:5<487::AID-EQE738>3.0.CO;2-M

Jankowski, R., Wilde, K. and Fujino, Y. (2000), "Reduction of pounding effects in elevated bridges during earthquakes", *Earthq. Eng. Struct. D*, **29**(2), 195-212. https://doi.org/10.1002/(sici)1096-9845(200002)29:2<195::aid-eqe897>3.0.co;2-3

Jiang, L., Feng, Y., Zhou, W. and He, B. (2019a), "Vibration characteristic analysis of high-speed railway simply supported beam bridge-track structure system", *Steel Compos. Struct., Int. J.*, **31**(6), 591-600. https://doi.org/10.12989/scs.2019.31.6.591

Jiang, L., Zhang, Y., Feng, Y., Zhou, W. and Tan, Z. (2019b), "Dynamic response analysis of a simply supported double-beam system under successive moving loads", *Appl. Sci.*, **9**(10), 2162. https://doi.org/10.3390/app9102162

Ju, S.H. (2012), "Nonlinear analysis of high-speed trains moving on bridges during earthquakes", *Nonlinear Dyn.*, **69**(1-2), 173-183. https://doi.org/10.1007/s11071-011-0254-5

Kang, X., Jiang, L., Bai, Y. and Caprani, C.C. (2017), "Seismic damage evaluation of high-speed railway bridge components under different intensities of earthquake excitations", *Eng. Struct.*, **152**, 116-128. https://doi.org/10.1016/j.engstruct.2017.08.057

Lai, M.H. and Ho, J.C.M. (2014), "Confinement effect of ring-confined concrete-filled-steel-tube columns under uni-axial load", *Eng. Struct.*, **67**, 123-141. https://doi.org/10.1016/j.engstruct.2014.02.013

Li, Y. and Conte, J.P. (2016), "Effects of seismic isolation on the seismic response of a California high-speed rail prototype bridge with soil-structure and track-structure interactions", *Earthq. Eng. Struct. D.*, **45**(15), 2415-2434. https://doi.org/10.1002/eqe.2770

Liu, X. and Ni, Y. (2018), "Wheel tread defect detection for high-speed trains using FBG-based online monitoring techniques", *Smart Struct. Syst., Int. J.*, **21**(5), 687-694. https://doi.org/10.12989/sss.2018.21.5.687

Liu, X., Xiang, P., Jiang, L., Lai, Z., Zhou, T. and Chen, Y. (2019), "Stochastic Analysis of Train-bridge System Using the Karhunen-Loéve Expansion and the Point Estimate Method", *Int. J. Struct. Stabil. Dyn.*, **20**(2), 2050025. https://doi.org/10.1142/S021945542050025X

Maragakis, E., Douglas, B.M., Haque, S. and Sharma, V. (1996), "Full-Scale Resonance Tests of a Railway Bridge", *Build. Int. Commun. Struct. Engrs.*, **1**(1), 183-190.

Montenegro, P.A., Calçada, R., Vila Pouca, N. and Tanabe, M. (2016), "Running safety assessment of trains moving over bridges subjected to moderate earthquakes", *Earthq. Eng. Struct.*, **45**(3), 483-504. https://doi.org/10.1002/eqe.2673

Montenegro, P.A., Barbosa, D., Carvalho, H. and Calçada, R. (2020a), "Dynamic effects on a train-bridge system caused by stochastically generated turbulent wind fields", *Eng. Struct.*, **211**, 110430. https://doi.org/10.1016/j.engstruct.2020.110430

Montenegro, P.A., Calçada, R., Carvalho, H., Bolkovoy, A. and Chebykin, I. (2020b), "Stability of a train running over the Volga river high-speed railway bridge during crosswinds",

Struct. *Infrastruct*. *Eng*., **16**(8), 1121-1137. https://doi.org/10.1080/15732479.2019.1684956

Shan, Y., Shu, Y. and Zhou, S. (2017), "Finite-infinite element coupled analysis on the influence of material parameters on the dynamic properties of transition zones", *Constr*. *Build*. *Mater*., **148**, 548-558. https://doi.org/10.1016/j.conbuildmat.2017.05.071

Toyooka, A., Ikeda, M., Yanagawa, H., Kataoka, H., Iemura, H. and Murata, K. (2005), "Effects of track structure on seismic behavior of isolation system bridges", *Quarterly Report of RTRI*, **46**(4), 238-243. https://doi.org/10.2219/rtriqr.46.238

Wei, B., Li, C., Jia, X., He, X. and Yang, M. (2019), "Effects of shear keys on seismic performance of an isolation system", *Smart Struct*. *Syst*., *Int*. *J*., **24**(3), 345-360. https://doi.org//10.12989/sss.2016.18.1.053

Wei, B., Hu, Z., He, X. and Jiang, L. (2020), "Evaluation of optimal ground motion intensity measures and seismic fragility analysis of a multi-pylon cable-stayed bridge with super-high piers in Mountainous Areas", *Soil Dyn*. *Earthq*. *Eng*., **129**, 105945. https://doi.org/10.1016/j.soildyn.2019.105945

Yan, B., Liu, S., Pu, H., Dai, G. and Cai, X. (2017), "Elastic-plastic seismic response of CRTS II slab ballastless track system on high-speed railway bridges", *Sci*. *China Technol*. *Sci*., **60**(6), 865-871. https://doi.org//10.1007/s11431-016-0222-6

Yan, W., Zhao, M., Sun, Q. and Ren, W. (2019), "Transmissibility-based system identification for structural health Monitoring: Fundamentals, approaches, and applications", *Mech*. *Syst*. *Signal Process*., **117**, 453-482. https://doi.org/10.1016/j.ymssp.2018.06.053

Zanardo, G., Hong, H. and Modena, C. (2010), "Seismic response of multi-span simply supported bridges to spatially varying earthquake ground motion", *Earthq*. *Eng*. *Struct*. *D*, **31**(6), 1325-1345. https://doi.org/10.1002/eqe.166

Zhai, W., Han, Z., Chen, Z., Ling, L. and Zhu, S. (2019), "Train-track-bridge dynamic interaction: a state-of-the-art review", *Vehicle Syst*. *Dyn*., **57**(7), 984-1027. https://doi.org/10.1080/00423114.2019.1605085

Zhang, Y.L., Wang, P.S. and Zhao, J.D. (2014), "Effects of CRTS II unballasted track on seismic response of high-speed railway bridge", *Appl*. *Mech*. *Mater*., **584-586**, 2099-2104. https://doi.org/10.4028/www.scientific.net/AMM.584-586.2099

Zhang, Y., Jiang, L., Zhou, W., Feng, Y., Tan, Z. and Chai, X. (2020), "Study of bridge-subgrade longitudinal constraint range for high-speed railway simply-supported beam bridge with CRTSII ballastless track under earthquake excitation", *Constr*. *Build*. *Mater*., **241**, 118026. https://doi.org/10.1016/j.conbuildmat.2020.118026